

---

# ADVERSARIAL ROBUSTNESS WITH NON-UNIFORM PERTURBATIONS

---

A PREPRINT

<b>Ecenaz Erdemir</b> <sup>*</sup> Imperial College London e.erdemir17@imperial.ac.uk	<b>Jeffrey Bickford</b> Amazon Web Services jbick@amazon.com	<b>Luca Melis</b> Amazon Web Services lucmeli@amazon.com	<b>Sergül Aydöre</b> Amazon Web Services saydore@amazon.com
---	--	--	---

## ABSTRACT

Robustness of machine learning models is critical for security related applications, where real-world adversaries are uniquely focused on evading neural network based detectors. Prior work mainly focus on crafting adversarial examples with small uniform norm-bounded perturbations across features to maintain the requirement of imperceptibility. Although such approaches are valid for images, uniform perturbations do not result in realistic adversarial examples in domains such as malware, finance, and social networks. For these types of applications, features typically have some semantically meaningful dependencies. The key idea of our proposed approach is to enable non-uniform perturbations that can adequately represent these feature dependencies during adversarial training. We propose using characteristics of the empirical data distribution, both on correlations between the features and the importance of the features themselves. Using experimental datasets for malware classification, credit risk prediction, and spam detection, we show that our approach is more robust to real-world attacks. Our approach can be adapted to other domains where non-uniform perturbations more accurately represent realistic adversarial examples.

## 1 Introduction

Deep neural networks (DNNs) are commonly used in a wide-variety of security-critical applications such as self-driving cars, spam detection, malware detection and medical diagnosis Madry et al. (2017). However, DNNs have been shown to be vulnerable to adversarial examples (AEs), which are perturbed inputs designed to fool the machine learning systems (Biggio et al., 2013; Szegedy et al., 2013; Goodfellow et al., 2014). To mitigate this problem, a line of research has focused on adversarial robustness of DNNs as well as the certification of these methods (Dvijotham et al., 2018; Gehr et al., 2018; Singh et al., 2018; Madry et al., 2017; Raghunathan et al., 2018; Wong & Kolter, 2018b; Zhang et al., 2018).

Adversarial training is one of the most effective empirical defenses against adversarial attacks (Kurakin et al., 2016; Madry et al., 2017). The goal during training is to minimize the loss of the DNN when perturbed samples are used. This way, the model becomes robust to real-world adversarial attacks. Though these empirical defenses do not provide theoretically provable guarantees, they have been shown to be robust against the strongest known attacks Wong et al. (2020). Some of the most common state-of-the-art adversarial attacks, such as projected gradient descent (PGD) Madry et al. (2017) and fast gradient sign method (FGSM) Wong et al. (2020), perturb training samples under a norm-ball constraint to maximize the loss of the network. The goal of certification, on the other hand, is to report whether an AE exists within an  $\ell_p$  norm centered at a given sample with a fixed radius. Certified defense approaches introduce theoretical robustness guarantees against norm-bounded perturbations (Wong & Kolter, 2018b; Raghunathan et al., 2018; Wang et al., 2018; Mirman et al., 2018).

In the computer vision domain, the adversary’s goal is to generate perturbed images that cause misclassifications in a DNN. It is often assumed that limiting a uniform norm-ball constraint results in perturbations that are imperceptible to the human eye. However in other applications such as fraud detection Zeager et al. (2017), spam detection Liu

---

<sup>\*</sup>Work done at Amazon Web Services.

et al. (2018b), credit card default prediction (Ballet et al., 2019; Levy et al., 2020) and malware detection (Li & Li, 2020; Pierazzi et al., 2020; Rosenberg et al., 2020), norm-bounded uniform perturbations may result in unrealistic transformations. Perturbed samples must comply with certain constraints related to the domain, hence preventing us from borrowing these assumptions from computer vision. These constraints can be on semantically meaningful feature dependencies, expert knowledge of possible attacks, and immutable features Guo et al. (2018); Pierazzi et al. (2020). This paper proposes a methodology to generate non-uniform perturbations that takes into account the characteristics of the empirical data distribution. Our results demonstrate that these non-uniform perturbations outperform uniform norm-ball constraints in these types of applications.

## 1.1 Background and Motivation

Adversarial training can be represented as a *min-max optimization* problem. Given a dataset  $\{x_i, y_i\}_{i=1}^n$  with input  $x_i \in \mathbb{R}^d$  and classes  $y_i \in \mathcal{Y}$ , the objective of adversarial training is denoted by

$$\min_{\theta} \frac{1}{n} \sum_{i=1}^n \max_{\delta \in \Delta} \ell(f_{\theta}(x_i + \delta), y_i) \quad (1)$$

where  $f_{\theta} : \mathbb{R}^d \rightarrow \mathcal{Y}$  is DNN function,  $\ell(\cdot)$  is the loss, e.g. cross-entropy, and  $\Delta$  is the set of possible adversarial perturbations around the original samples. The adversary's objective is the inner maximization term in equation 1, and the perturbed samples found as a solution to the norm-constrained inner maximization are called adversarial examples, or AEs.

Consider the 2D toy example of binary classification in Figure 1 which is obtained by modifying Wong & Kolter (2018a). Figure 1 illustrates adversarially robust decision boundaries with red and blue regions, and  $l_2$ -norm perturbation limits around the data points with black circles. While Figure 1a shows that adversarially trained model with input constraint  $\|\delta\|_2 \leq 0.5$  gains complete robustness against input perturbations, in Figure 1b there is loss of clean performance due to overlapping regions of increased allowed perturbations. Although the constraint  $\|\delta\|_2 \leq 0.5$  might provide sufficient robustness in  $x$ -axis, there are still uncovered regions in  $y$ -axis in Figure 1a. On the other hand, when we fit the allowable perturbations to  $y$ -axis by choosing a larger perturbation  $\|\delta\|_2 \leq 0.8$ ,  $x$ -axis suffers from unnecessary overlaps. This can be solved by customizing the perturbation constraint such that  $\|\delta_x\|_2 \leq 0.5$  and  $\|\delta_y\|_2 \leq 0.8$  which results in an ellipsoid perturbation region in 2D as shown in Figure 1c. This toy example highlights the advantage of a non-uniform constraint across both axes.

The intuition behind the need for non-uniform constraints is apparent across many industrial applications. A common cybersecurity application is malware detection, which identifies if an executable file is benign or malicious. Unlike images, diverse and semantically meaningful features are extracted from the executable file and are passed to a machine learning model. To maintain the functionality of an executable file during an adversarial attack, certain features may be immutable and perturbations may result in an unrealistic scenario. For example in the Android malware space, application permissions, such as permission to access a phone's location service, are required for malicious functionality and cannot be perturbed Li & Li (2020). In a finance scenario where customer credit card applications are evaluated by machine learning models, a possible set of features include age, gender, income, savings, education level, number of dependents, etc. In this type of dataset there are clear dependencies between features, for example the number of dependents has a meaningful correlation with age. When detecting spammers within social networks, features are extracted from accounts and may include the length of the username, length of user description, number of following and followers as well as the ratio between them, percentage of bidirectional friends, number of posted messages per day, etc. Similar to the previous finance example, there is a meaningful correlation between features such as the percentage of bidirectional friends and the ratio of followers.

In all of these scenarios, non-uniform perturbations can be used to maintain these correlations and semantically meaningful dependencies resulting in more realistic adversarial samples. In this work, we propose adversarial training with these more realistic perturbations to increase the robustness against real-world adversarial attacks. Specifically, our contributions are: (i) Instead of considering an allowed perturbation region where all the features are treated uniformly, i.e.,  $\|\delta\|_p \leq \epsilon$ , we consider a transformed input perturbation constraint, i.e.,  $\|\Omega\delta\|_p \leq \epsilon$  where  $\Omega$  is a transformation matrix, which takes the available information into account, such as feature importance, feature correlations and/or domain knowledge. Hence, the transformation in the norm ball constraint results in non-uniform input perturbations over the features. (ii) For various applications such as malware detection, credit risk prediction and spam detection, we show that robustness using non-uniform perturbations outperforms the commonly-used uniform approach. (iii) To provide provable guarantees for non-uniform robustness, we modify two known certification methods, linear programming and randomized smoothing, to account for non-uniform perturbation constraints.

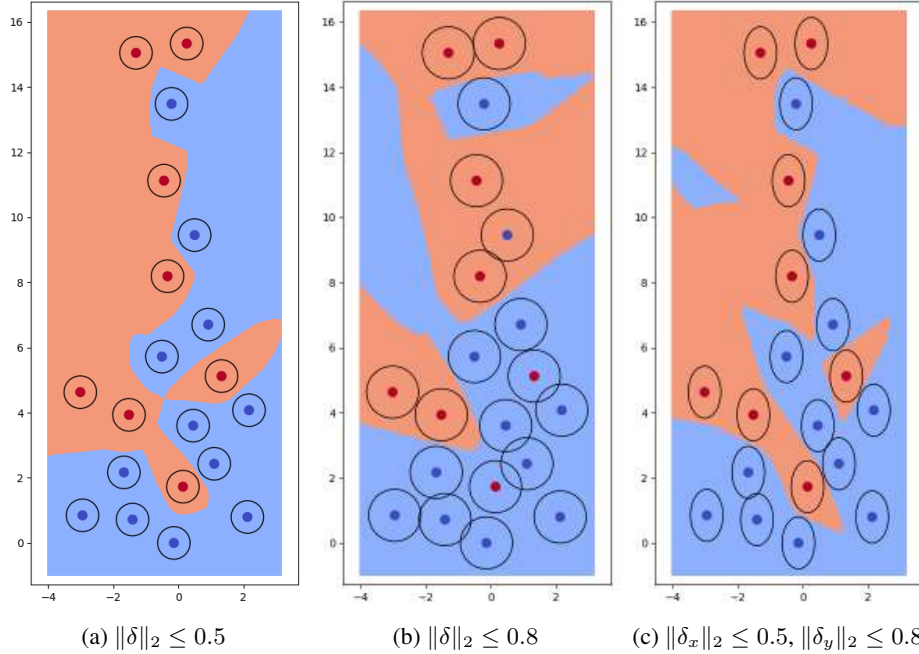


Figure 1: Classification boundaries from adversarial training with uniform perturbation limits for (a)  $\|\delta\|_2 \leq 0.5$ , (b)  $\|\delta\|_2 \leq 0.8$  and non-uniform perturbation limits for (c)  $\|\delta_x\|_2 \leq 0.5$  and  $\|\delta_y\|_2 \leq 0.8$ .

## 2 Related Work

The approach of applying different levels of robustness for different features has already been studied in the literature Tsipras et al. (2018); Ilyas et al. (2019); Liu et al. (2019). Among these, Tsipras et al. (2018) and Ilyas et al. (2019) study the effect of robust and non-robust features in standard and adversarial training. Both works show that different types of features might have different levels of robustness against small input perturbations. This can also be interpreted as different levels of perturbation tolerance of features which is the core idea of our approach.

A closely related work to ours is Liu et al. (2019) which considers non-uniform perturbation bounds for input features. Given a non-uniform adversarial budget  $\epsilon$  for  $\ell_\infty$  norm bounded inputs, Liu et al. (2019) proposes a framework that maximizes the volumes of certified bounds. However, this work only proposes robustness certification of pre-trained models, and does not consider training a robust model against these non-uniform perturbations. The approach is also data-agnostic meaning that it does not take correlations or an additional knowledge on the data into account. We instead use non-uniform perturbations in data-dependent adversarial training to achieve robustness in a DNN model. In fact, Liu et al. (2019) mentioned consideration of feature correlations as a potential future direction of their work.

In Wong & Kolter (2020), a conditional variational autoencoder (CVAE) is trained to learn perturbation sets for image data and the generated adversarial images are then used in augmented training. The work proposes robustness against common image corruptions as well as  $\ell_p$  perturbations. However, it mainly focuses on possible corruptions and attacks specific to image domain, and assumes access to the test data distribution. In our work, we focus on non-image data which have correlated and different scale features and we do not rely on an additional knowledge of the test set.

Recent work in the malware detection space Pierazzi et al. (2020) creates realistic adversarial samples by defining a set of comprehensive and realistic constraints on how an input file can be transformed. Though this approach creates realistic adversarial samples, collecting a representative corpus of raw input files is a challenging problem Pendlebury et al. (2019). The recent release of binary feature sets, such as the EMBER dataset Anderson & Roth (2018), enables model development without having access to the raw input files. Our work can be used to create more realistic adversarial examples in situations where access to a large representative corpus of files is not possible.

### 3 Non-uniform Adversarial Perturbations

In adversarial training, the worst case loss for an allowed perturbation region is minimized over parameters of a function representing a neural network as presented in equation 1. The objective of the adversary can be written as the inner maximization of equation (1):

$$\underset{\delta \in \Delta_{\epsilon,p}}{\text{maximize}} \quad \ell(f_\theta(x + \delta), y) \quad (2)$$

where  $\Delta_{\epsilon,p} = \{\delta : \|\delta\|_p \leq \epsilon\}$  is an  $\ell_p$  ball of radius  $\epsilon$  which defines the feasible perturbation region.

Standard PGD follows steepest descent which iteratively updates  $\delta$  in the gradient direction to increase the loss:

$$\delta^{t+1} = \delta^t + \alpha \frac{\nabla_\delta \ell(f_\theta(x + \delta^t), y)}{\|\nabla_\delta \ell(f_\theta(x + \delta^t), y)\|_p} \quad (3)$$

at iteration  $t$ , and then it projects  $\delta$  to the closest point onto the  $\ell_p$  ball:

$$\mathcal{P}_{\Delta_{\epsilon,p}}(\delta) := \arg \min_{\delta' \in \Delta_{\epsilon,p}} \|\delta - \delta'\|_2^2 \quad (4)$$

where the distance between  $\delta$  and  $\delta'$  is the Euclidean distance. This projection corresponds to normalizing  $\delta$  to have a maximum  $\ell_p$  norm which is equal to  $\epsilon$ , that is,

$$\mathcal{P}_{\Delta_{\epsilon,p}}(\delta) = \epsilon \frac{\delta}{\max\{\epsilon, \|\delta\|_p\}}. \quad (5)$$

#### 3.1 Non-uniform Perturbation Set

Here, we introduce an adversarial constraint set that non-uniformly limits adversarial variations in different, potentially correlated dimensions, by

$$\tilde{\Delta}_{\epsilon,p} = \{\delta : \|\Omega\delta\|_p \leq \epsilon\} \quad (6)$$

where  $\Omega \in \mathbb{R}^{d \times d}$ . In our approach,  $\delta$  is updated by equation (3) similar to the standard PGD, however, it is projected back to a non-uniform norm ball satisfying  $\|\Omega\delta\|_p \leq \epsilon$ . The corresponding projection operator will then be:

$$\mathcal{P}_{\tilde{\Delta}_{\epsilon,p}}(\Omega\delta) = \begin{cases} \epsilon \frac{\delta}{\|\Omega\delta\|_p} & \text{if } \|\Omega\delta\|_p > \epsilon \\ \delta & \text{otherwise.} \end{cases} \quad (7)$$

The choice of  $\Omega$  depends on how we model the expert knowledge or feature relationships. The following are our choices for the non-uniform perturbation sets.

##### 3.1.1 Mahalanobis Distance

Euclidean distance between two points in a multi-dimensional space is a useful metric when the vectors have isotropic distribution (i.e. radially symmetric). This is because the Euclidean distance assumes each dimension have same scale (or spread) and are uncorrelated to other dimensions. However, isotropy is usually not the case for real datasets in which different features might have different scales and can be correlated. Fortunately, Mahalanobis distance accounts for how the features are scaled and correlated to one another. Therefore, it is a more useful metric if the data of interest has non-isotropic distribution.

Mahalanobis distance is initially defined as the  $\ell_2$  distance between a point and a distribution Mahalanobis (1936). It is also used to measure dissimilarity between two vectors from the same distribution. By formal definition, Mahalanobis distance between vectors  $z, z' \in \mathbb{R}^d$  is denoted by

$$d_M(z, z' | M) := \sqrt{(z - z')^T M (z - z')} \quad (8)$$

where  $M \in \mathbb{R}^{d \times d}$  is a positive semi-definite matrix which can be decomposed as  $M = U^T U$ , for  $U \in \mathbb{R}^{d \times d}$ . The dissimilarity between two vectors from a distribution with covariance  $\Sigma$  can be measured by selecting  $M = \Sigma^{-1}$ . If feature vectors of a dataset are uncorrelated and have unit variances, their covariance matrix is  $\Sigma = I$ , which reduces their Mahalanobis distance to Euclidean distance.

We are interested in the distance between the original sample and the perturbed sample. Since we assume all perturbations are additive, as common practice, the distance term we consider is  $\sqrt{\delta^T M \delta}$ . For a generalized Mahalanobis distance in

$\ell_p$  norm, selecting  $\Omega = U^T$  corresponds to the perturbation set  $\tilde{\Delta}_{\epsilon,p} = \{\delta : \|U^T\delta\|_p \leq \epsilon\}$  which generates AEs with feature correlations similar to the original dataset.

Robustness of an adversarially trained model is directly related to how realistic the generated AEs are during training. Now, we explore implications of selecting  $\ell_2$  Mahalanobis distance to define the limits of the perturbation set. To ensure the validity of the AEs, we consider the notion of consistency of the generated sample with real samples. Levy et al. (2020) introduced the notion of  $\epsilon$ -inconsistency to quantify how likely an AE is. With slight change in their notation, we define  $\gamma$ -consistency as follows:

**Definition 3.1.** For a consistency threshold  $\gamma \in [0, 1]$ , an AE is  $\gamma$ -consistent if

$$\mathbb{P}(X = x \mid y) \geq \gamma, \quad (9)$$

where  $\mathbb{P}$  is a conditional Gaussian distribution with zero mean and covariance matrix  $\Sigma_y$ .

**Theorem 3.1.**  $\gamma$ -consistency of the AEs generated under Mahalanobis distance constraint has a direct relation to  $\epsilon$  such that

$$\sqrt{2C - 2 \log \gamma} \leq \epsilon. \quad (10)$$

where  $C = -\log(2\pi)^{d/2} |\Sigma_y|^{1/2}$ ,  $d$  is the dimension of  $x$ , and  $\sqrt{\delta^T \Sigma_y^{-1} \delta} \leq \epsilon$ .

Theorem 3.1 implies that there is a direct relationship between limiting the Mahalanobis distance of  $\delta$  and ensuring consistent samples when the data is Gaussian. In other words, when the  $\ell_2$  Mahalanobis distance of the perturbations gets smaller, AEs become more consistent. See Appendix 7.2 for the proof.

### 3.1.2 Weighted Norm

When  $\Omega$  is a diagonal matrix, inner maximization constraint simply becomes the weighted norm of  $\delta$  limited by  $\epsilon$ , and the weights are denoted by  $\{\Omega_{i,i}\}_{i=1}^d$ . Projection of  $\delta$  under the new constraint corresponds to projection onto an  $\ell_p$  norm ball of radius  $\frac{\epsilon}{\Omega_{i,i}}$  for  $i^{th}$  feature. These weights can be chosen exploiting domain, attack or model knowledge. For instance, more important features can be allowed to be perturbed more than the other features which have less effect on the output score of the classifier. This knowledge might come from Pearson's correlation coefficients Ballet et al. (2019) between the features of the training data and the corresponding labels, or Shapley values Shapley (1951) for each feature.

Using Pearson's correlation coefficient of each feature with the corresponding target variable, i.e.,  $|\rho_{i,y}|$  for  $i^{th}$  feature and output  $y$ , we let larger perturbation radii for more correlated features with the output. Due to the inverse relation between  $\Omega_{i,i}$  and the radius of the ball, for  $\bar{\rho}_{i,y} = \frac{1}{|\rho_{i,y}|}$  we select  $\Omega$  as  $\Omega = \frac{\text{diag}(\{\bar{\rho}_{i,y}\}_{i=1}^d)}{\|\{\bar{\rho}_{i,y}\}_{i=1}^d\|_2}$ . Similarly, using Shapley values to represent feature importance, we define  $s_i$  as the Shapley value of feature  $i$  and  $\bar{s}_i = \frac{1}{|s_i|}$ , following the intuition that more important features should have larger perturbation radii, we choose  $\Omega$  as  $\Omega = \frac{\text{diag}(\{\bar{s}_i\}_{i=1}^d)}{\|\{\bar{s}_i\}_{i=1}^d\|_2}$ .

In the malware domain, expert knowledge might help to rule out specific type of attacks crafted on immutable features due to feasibility constraints. This can be modelled by the proposed weighted norm constraint as masking the perturbations on immutable features. Hence, non-uniform perturbation approach enables various transformations on the attack space to gain robustness against realistic attacks.

## 4 Experimental Results

In this section, we present experimental results to evaluate robustness of DNNs against adversarial attacks for binary classification problems on three applications: malware detection, credit risk prediction, and spam detection. We compare PGD with non-uniform perturbations during adversarial training with the standard PGD based on uniform perturbations. For all applications, we evaluate our defense mechanisms on adversarial attacks proposed by other works. Although we only consider binary classification problems in this work, our approach can be adapted to multi-dimensional classification problems.

For all applications, we use a fully-connected neural network model composed of four densely connected layers with the first three using *ReLU* activations followed by a *softmax* activation in the last layer. After each of the first three layers, we apply  $\%20$  *Dropout* rate for regularization during training. We use 5 random initialization for malware and 10 for both credit risk and spam detection use-cases to report average results. Note that our goal is not to design the best possible neural network but instead compare various perturbations during adversarial training for a given DNN.

We use standardization as a normalization method for all use-cases. Normalization as a pre-processing step is a common practice with many machine learning techniques. Min-max scaling transforms all features into the same scale while standardization, which is the recommended approach in presence of outliers Han et al. (2011), only ensures zero mean and unit standard deviation. This approach does not guarantee same range (min and max) for all features. As a result, it is possible that the features have different scales even after normalization.

**Adversarial training:** We perform adversarial training in all use-cases by applying  $\ell_2$ -norm PGD for uniform perturbation sets, i.e.,  $\Delta_{\epsilon_1,2} = \{\delta : \|\delta\|_2 \leq \epsilon_1\}$ , and non-uniform perturbation sets, i.e.,  $\tilde{\Delta}_{\epsilon_2,2} = \{\delta : \|\Omega\delta\|_2 \leq \epsilon_2\}$ . Since potential adversaries are not interested in fooling the classifiers with negative class (target class) samples,  $\delta$  perturbations are only applied to the positive classes during adversarial training. Positive classes are the malicious class in malware detection, bad class in credit risk prediction, and spammer class in spam detection. Moreover, for the sake of clean accuracy within the positive class, adversarial perturbations are applied to %90 of the positive samples during training.

To model the expert knowledge with diagonal  $\Omega$ , we use Pearson’s correlation coefficient, Shapley values as introduced in Section 3.1, and masking to allow perturbation only in mutable features. To compute Shapley values, we use SHAP (SHapley Additive exPlanations) Lundberg & Lee (2017) which utilizes a deep learning explainer.

We also consider adversarial training under the Mahalanobis distance (MD) constraint introduced in Section 3.1. We select  $\Omega = U^T$  for  $U^T U = \Sigma_y^{-1}$  considering two cases;  $\Sigma_y$  is the covariance matrix calculated from the entire training data, i.e.,  $y = \{0, 1\}$ , and  $\Sigma_y$  is only for the negative (target) class  $y = 0$ .

We call the adversarially trained models with non-uniform perturbations according to their  $\Omega$  selection, e.g., *NU- $\delta$ -Pearson* for Pearson’s correlation coefficients, *NU- $\delta$ -SHAP* for Shapley values, *NU- $\delta$ -Mask* for masking, *NU- $\delta$ -MD* for Mahalanobis distance using full covariance matrix and *NU- $\delta$ -MDtarget* for Mahalanobis distance using the covariance matrix of only negative class. The choice of  $\Omega = I$  corresponds to adversarial training with uniform perturbation constraints, which we call *Uniform- $\delta$* .

#### 4.1 Malware Use-case

First, we consider a binary classification problem for malware detection using the EMBER dataset Anderson & Roth (2018). EMBER is a feature-based public dataset which is considered a benchmark for Windows malware detection. It contains 2381 features extracted from Windows PE files: 600K labeled training samples (300K malicious, 300K benign) and 200K test samples (100K malicious, 100K benign). We refer to Appendix 7.1 for more detailed description of the EMBER dataset features. Given a malware sample, an adversary’s goal is to make the DNN conclude that a malicious sample is benign.

**Attacks used for evaluation:** In the malware domain, test-time evasion attacks can be classified as *feature-space* and *problem-space* attacks. While the former crafts AEs by modifying the features extracted from binary files, the latter directly modifies malware binaries making sure of the validity and inconspicuousness of the modified object. We evaluate the robustness of our model against evasion attacks which are crafted in problem-space, i.e., on PE files. We incorporate the most successful attacks Fleshman (2019) from the machine learning static evasion competition of DEFCON (2019). Since the EMBER dataset only contains the extracted features of a file, a subset of malware binaries used for AE generation are obtained from VirusTotal VirusTotal using the SHA256 hash as an identifier.

We observe that these problem-space attacks, which add various bytes to a file without modifying the core functionality, affect only the feature groups “Byte Histogram”, “Byte Entropy Histogram” and “Section Information”. Experts aware of these byte padding attacks understand which features can be manipulated by an attacker. In addition to the previous adversarial training methods, we represent this *best case expert knowledge* by  $\Omega = I_{mask}$ , which is an identity matrix with non-zero diagonal elements only for “Byte Histogram”, “Byte Entropy Histogram” and “Section Information” features. That is, the model is adversarially trained with PGD perturbations applied only to these specific features, and we call it *NU- $\delta$ -Mask*.

**Numeric results:** We present clean accuracy and defense success rate in Table 2 and a detailed breakdown of number of evasions by each problem-space attack in Table 1 in Appendix. To make a fair comparison between uniform and non-uniform approaches,  $\epsilon$  for each method is selected such that their average  $\|\delta\|_2$  are approximately equal. We test the detection success of adversarially trained models with 9000 AE sets generated by the problem-space attacks described in Appendix 7.3. In Table 2, “Clean Ac.” shows the model performance on clean EMBER test data, while “Defense S.R.” represents the success rate of the model in detecting 9000 AEs. Defense S. R. is the average performance of the model against various problem-space attacks. We refer to Table 7.1 for detailed attack performances. The results show that as the average perturbation  $\|\delta\|_2$  increases, adversarially trained models become more robust against problem-space attacks up to a point between  $\|\delta\|_2 \in [11, 18]$  while slightly loosing their clean accuracy. After that point, both clean

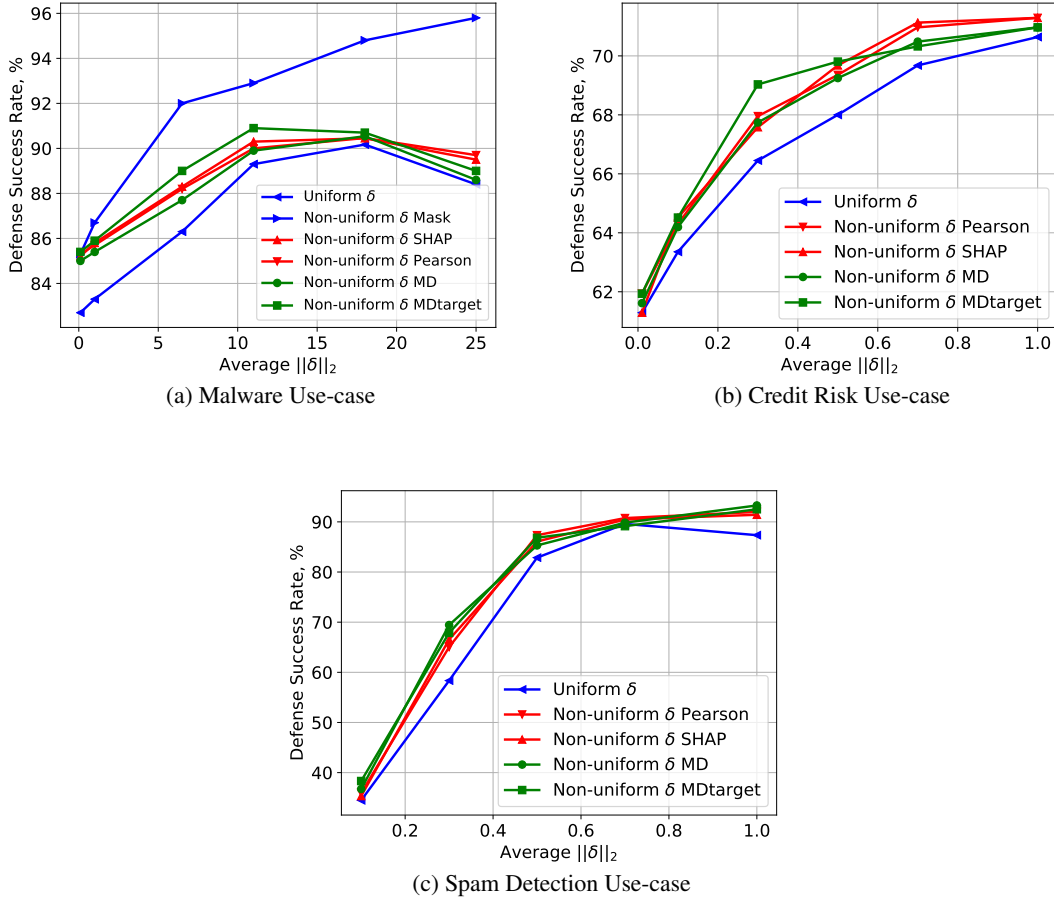


Figure 2: Defense success rate of  $\ell_2$ -PGD adversarial trainings against the problem-space attacks, where all non-uniform perturbation defense approaches outperform the uniform perturbation approach for all use-cases.

accuracy and defense success rate start decreasing in all models except *NU- $\delta$ -Mask*. Figure 2a illustrates the defense success rate on Table 2 and shows that non-uniform perturbation approaches outperform the uniform perturbation in all cases. Moreover, *NU- $\delta$ -MDtarget* performs closest to the best case expert knowledge *NU- $\delta$ -Mask* for all cases except when  $\|\delta\|_2 = 25$ . The advantage of selecting  $\Sigma$  from benign samples versus selecting from the entire dataset is that the direction of perturbations are led towards the target class, i.e. benign samples, for *NU- $\delta$ -MDtarget*. We also do not observe a significant performance difference between *NU- $\delta$ -Pearson* and *NU- $\delta$ -SHAP*, while *NU- $\delta$ -MD* only differs from the two for  $\|\delta\|_2 = 25$ .

#### 4.2 Credit Risk Use-case

Our second use-case is a binary credit risk classification problem where the DNN’s goal is to make decisions on loan applications for bank customers. For this scenario, we use the well known German Credit dataset Merz & Murphy (1996), which contains classes “good” and “bad”, as well as applicant features such as age, employment status, income, savings, etc. It has 20 features and 1000 samples with 300 belonging to the “bad” class. Similar to Ballet et al. (2019), we treat discrete features as continuous and drop non-ordinal categorical features.

**Attacks used for evaluation:** The goal of an adversary in this situation is to make DNN models conclude that they are approved for a loan when they actually may not be eligible. Since modifications to tabular data can be detected by an expert eye, attackers try to fool classifiers with imperceptible attacks. We use German Credit dataset implementation of LowProFool Ballet et al. (2019) which considers attack imperceptibility and represents expert knowledge using feature correlations. We apply the attack on the “bad” class of the test set and generate 155 AEs. After dropping the non-ordinal categorical features, we treat the remaining 12 features as continuous values.

**Numeric results:** In Table 3, we present clean accuracy and defense success rate of PGD with uniform and non-uniform perturbations against LowProFool. Similar to the malware use-case,  $\epsilon$  for each method is selected such that their average  $\|\delta\|_2$  are approximately equal. Table 3 shows accuracy of the model tested with clean German Credit test data (Clean Ac.), and the success rate of the model in detecting 155 AEs generated by LowProFool (Defense S.R.). We observe a consistent increase in the defense success rate, i.e. robustness against the attack, as average  $\|\delta\|_2$  increases. The only decrease occurs for  $NU\text{-}\delta\text{-}MDtarget$  after the point  $\|\delta\|_2 = 1.5$ . On the other hand, clean accuracy decreases with the increasing amount of perturbation applied during adversarial training. Summary of results in Table 3 are illustrated in Figure 2b showing that for every given  $\|\delta\|_2$ , non-uniform perturbations outperform uniform perturbations in PGD. Although LowProFool represents feature importance by Pearson correlation coefficients between features and the output score, surprisingly  $NU\text{-}\delta\text{-}Pearson$  is the best approach among the other non-uniform approaches for only  $\delta = \{0.7, 1\}$ .

### 4.3 Spam Detection Use-case

Finally, we evaluate robustness within the context of detecting spam within social networks. We use a dataset from Twitter, where data from legitimate users and spammers is harvested from social honeypots over seven months Lee et al. (2011). This dataset contains profile information and posts of both spammers and legitimate users. After pre-processing Huang (2017), we extract 31 numeric features with 14 being integers and the rest being continuous. Some examples of these features are the number of following and followers as well as the ratio between them, percentage of bidirectional friends, number of posted messages per day, etc. We treat all features as continuous values in our experiments. Moreover, we extract 41,354 samples where the training set has 17,744 “bad” and 15,339 “good” samples, and the testing set has 3885 “bad” and 4386 “good” samples. The goal of an adversary is to make the DNN predict that a tweet was posted by a legitimate user when in actuality it was written by a spammer.

**Attacks used for evaluation:** We incorporate the evasion attack Liu et al. (2018a) from Liu et al. (2018b) for our Twitter spam detector. The attack strategy is based on minimizing the maliciousness score of an AE which is measured by a local interpretation model LASSO, while satisfying  $\ell_2$  norm constraint on perturbations. We generate the AEs by constraining the perturbations to  $0.5 \times dist_{pos-neg}^{avg}$ , where  $dist_{pos-neg}^{avg}$  is defined by Liu et al. (2018b) as the average distance between the spammer samples and the closest non-spammers to these samples. We split the Twitter dataset with ratio %25 for training and testing, and generate the AEs using the spammer class of the entire test set.

**Numeric results:** Table 4 exhibits the clean test accuracy and defense success rate in detecting AEs of the proposed approaches against the model interpretation based attack Liu et al. (2018b) for Twitter dataset. As before, we apply perturbations only to the spammer set during adversarial training and show the experiments for approximately equal average  $\|\delta\|_2$  perturbations. Table 4 clearly shows that non-uniform perturbations outperform uniform case in terms of defense S.R. for all given  $\|\delta\|_2$ . This is also illustrated in Figure 2c. Moreover, defense success rate (S. R.) for  $Uniform\text{-}\delta$  decreases after the point  $\|\delta\|_2 = 0.7$ .

## 5 Certified Robustness with Non-uniform Perturbations

In this section, we present methods for certifying robustness with non-uniform perturbations. We consider two well known certification methods; a linear programming (LP) approach Wong & Kolter (2018b) and randomized smoothing Cohen et al. (2019).

### 5.1 LP Formulation

We can provably certify the robustness of deep ReLU networks against non-uniform adversarial perturbations at the input. Our derivation follows a linear programming formulation of the adversary’s problem with ReLU relaxations, then the dual problem of the linear program and activation bound calculation. It can be viewed as an extension of the work proposed by Wong & Kolter (2018b).

Similar to Wong & Kolter (2018b), we consider a  $k$  layer feedforward deep ReLU network with

$$\begin{aligned} \hat{z}_{i+1} &= W_i z_i + b_i, \text{ for } i = 1, \dots, k-1 \\ z_i &= \max\{\hat{z}_i, 0\}, \text{ for } i = 1, \dots, k-1 \end{aligned} \tag{11}$$

We denote  $\mathcal{Z}_{\epsilon, \Omega}(x) := \{f_\theta(x + \delta) : \|\Omega\delta\|_p \leq \epsilon\}$  as the set of all attainable final-layer activations by input perturbation  $\delta$ . Since this is a non-convex set for multi-layer networks which is hard to optimize over, we consider a convex outer bound on  $\mathcal{Z}_{\epsilon, \Omega}(x)$  and optimize the worst case loss over this bound to guarantee that no adversarial examples within  $\mathcal{Z}_{\epsilon, \Omega}(x)$  can evade the network. As done in Wong & Kolter (2018b), we relax the ReLU activations by representing

$z = \max\{0, \hat{z}\}$  with their upper convex envelopes

$$z \geq 0, z \geq \hat{z}, -u\hat{z} + (u - l)z \leq -ul, \quad (12)$$

where  $l$  and  $u$  are the known lower and upper bounds for the pre-ReLu activations. We denote the new relaxed set of all attainable final-layer activations by  $\tilde{\mathcal{Z}}_{\epsilon, \Omega}(x)$ . Assuming that an adversary targets a specific class to fool the classifier, we can write the linear program as

$$\underset{\hat{z}_k}{\text{minimize}} \quad c^T \hat{z}_k \quad \text{s.t.} \quad \hat{z}_k \in \tilde{\mathcal{Z}}_{\epsilon, \Omega} \quad (13)$$

where  $c := e_{y_{\text{true}}} - e_{y_{\text{target}}}$  is the difference between the selection vector of true class and the target class.

A positive valued objective for all classes as a solution to equation 13 indicates that there is no adversarial perturbation within  $\tilde{\Delta}_{\epsilon, p}$  which can evade the classifier. To be able to solve equation 13 in a tractable way, we consider its dual problem whose feasible solution provides a guaranteed lower bound for the LP. It is previously shown by (Wong & Kolter, 2018b) that a feasible set of the dual problem can be formulated similar to a standard backpropagation network and solved efficiently. The dual problem of our LP with ReLU relaxation and non-uniform perturbation constraints is expressed in the following theorem.

**Theorem 5.1.** *The dual of the linear program 13 can be written as*

$$\begin{aligned} \underset{\hat{\nu}, \nu}{\text{maximize}} \quad & -\sum_{i=1}^{k-1} \nu_{i+1}^T b_i + \sum_{i=2}^{k-1} \sum_{j \in \mathcal{I}_i} l_{i,j} [\hat{\nu}_{i,j}]_+ - \hat{\nu}_1^T x \\ & - \epsilon \|\Omega^{-1} \hat{\nu}_1\|_q \\ \text{s.t.} \quad & \nu_k = -c \\ & \hat{\nu}_i = (W_i^T \nu_{i+1}), i = k-1, \dots, 1 \\ & \nu_{i,j} = \begin{cases} 0 & j \in \mathcal{I}_i^- \\ \hat{\nu}_{i,j} & j \in \mathcal{I}_i^+ \\ \frac{u_{i,j}}{u_{i,j} - l_{i,j}} [\hat{\nu}_{i,j}]_+ - \eta_{i,j} [\hat{\nu}_{i,j}]_- & j \in \mathcal{I}_i \end{cases} \\ & i = k-1, \dots, 2 \end{aligned} \quad (14)$$

where  $\mathcal{I}_i^-$ ,  $\mathcal{I}_i^+$  and  $\mathcal{I}_i$  represent the activation sets in layer  $i$  for  $l$  and  $u$  are both negative, both positive and span zero, respectively.

See Appendix 7.2 for the proof of Theorem 5.1. When  $\eta_{i,j} = \frac{u_{i,j}}{u_{i,j} - l_{i,j}}$ , Theorem 5.1 shows that the dual problem can be represented as a linear back propagation network, which provides a tractable solution for a lower bound of the primal objective. To solve equation 14, we need to calculate lower and upper bounds for each layer incrementally as in the following part.

**Activation Bounds:** The dual objective function provides a bound on any linear function  $c^T \hat{z}_k$ . Therefore, we can compute the dual objective for  $c = -I$  and  $c = I$  to obtain lower and upper bounds. For  $c = I$ , value of  $\nu_i$  for all activations simultaneously is given by

$$\begin{aligned} \hat{\nu}_i &= W_i^T D_{i+1} W_{i+1}^T \dots D_n W_n^T \\ \nu_i &= D_i \hat{\nu}_i, \end{aligned} \quad (15)$$

where  $D_i$  is a diagonal matrix with

$$(D_i)_{jj} = \begin{cases} 0 & j \in \mathcal{I}_i^- \\ 1 & j \in \mathcal{I}_i^+ \\ \frac{u_{i,j}}{u_{i,j} - l_{i,j}} & j \in \mathcal{I}_i \end{cases} \quad (16)$$

Similar to Wong & Kolter (2018b), bounds for  $\nu_i$  and  $\hat{\nu}_i$  can be computed for each layer by cumulatively generating bounds for  $\hat{z}_2$ , then  $\hat{z}_3$  and so on. By initializing  $\hat{\nu}_1 := W_1^T$ ,  $\zeta_1 := b_1^T$ , first bounds are  $l_2 := x^T W_1^T + b_1^T - \epsilon \|\Omega^{-1} W_1^T\|_q$  and  $u_2 := x^T W_1^T + b_1^T + \epsilon \|\Omega^{-1} W_1^T\|_q$ , where the norms are taken over the columns. Calculation of the bounds for each layer is given in Algorithm 1.

For certification of robustness within a non-uniform norm ball around a test sample, we need the objective of the LP to be positive for all classes. Since the solution of the dual problem is a lower bound on the primal LP, it provides a worst case certification guarantee against the adversaries within the non-uniform norm ball. To support the approaches proposed in Section 3, we provide certification results for their robustness under both uniform and non-uniform norm ball constraints in Appendix 7.4. Our results show that certifying with non-uniform bounds results in larger certification margins and higher number of certified samples indicating tighter verification for non-uniform approach.

---

**Algorithm 1** Activation Bound Calculation

---

**Input:** Network parameters  $\{W_i, b_i\}$ , input data  $x$ , input constraint matrix  $\Omega$  and ball size  $\epsilon$ , norm type  $q$ .  
 Initialize  $\hat{\nu}_1 := W_1^T$ ,  $\zeta_1 := b_1^T$   
 $l_2 = x^T W_1^T + b_1^T - \epsilon \|\Omega^{-1} W_1^T\|_q$   
 $u_2 = x^T W_1^T + b_1^T + \epsilon \|\Omega^{-1} W_1^T\|_q$   
 $\nu_{2,\mathcal{I}_2} := (D_2)_{\mathcal{I}_2} W_2^T$   
 $\zeta_2 = b_2^T$   
**for**  $i = 2$  **to**  $k - 1$  **do**  
 $l_{i+1} = x^T \hat{\nu}_1 + \sum_{j=1}^i \zeta_j - \epsilon \|\Omega^{-1} \hat{\nu}_1\|_q + \sum_{\substack{i=2 \\ i' \in \mathcal{I}_i}}^i l_{j,i'} [-\nu_{j,i'}]_+$   
 $u_{i+1} = x^T \hat{\nu}_1 + \sum_{j=1}^i \zeta_j + \epsilon \|\Omega^{-1} \hat{\nu}_1\|_q - \sum_{\substack{i=2 \\ i' \in \mathcal{I}_i}}^i l_{j,i'} [\nu_{j,i'}]_+$   
 $\nu_{j,\mathcal{I}_j} = \nu_{j,\mathcal{I}_j} (D_i)_{\mathcal{I}_i} W_i^T$   
 $\zeta_j = \zeta_j D_i W_i^T$   
 $\hat{\nu}_1 = \hat{\nu}_1 (D_i)_{\mathcal{I}_i} W_i^T$   
**end for**  
**Output:**  $\{l_i, u_i\}_{i=2}^k$

---

## 5.2 Randomized Smoothing

Robustness certification via *randomized smoothing* Cohen et al. (2019) is an empirical alternative approach to the method discussed in Section 5.1. The idea is constructing a “smoothed” classifier  $g$  from the base classifier  $f$ . In the original formulation introduced in Cohen et al. (2019), the smoothed classifier  $g$  returns the most likely output returned by the base classifier  $f$  given input  $x$  is perturbed by isotropic Gaussian noise. Here, we provide robustness guarantee in binary case for randomized smoothing framework when non-isotropic Gaussian noise is used to allow robustness to non-uniform perturbations:

$$g(x) = \arg \max_{y \in \mathcal{Y}} \mathbb{P}(f(x + n) = y) \quad \text{where} \quad n \sim \mathcal{N}(0, \Sigma). \quad (17)$$

Adapting notation and Theorem 2 from Cohen et al. (2019), let  $p_a$  be the probability of the most probable class  $y = a$  when the base classifier  $f$  classifies  $\mathcal{N}(x, \Sigma)$ . Then the following theorem holds.

**Theorem 5.2.** *In binary classification problem, suppose  $\underline{p}_a \in (\frac{1}{2}, 1]$  satisfies  $\mathbb{P}(f(x+n) = a) \geq \underline{p}_a$ . Then  $g(x+\delta) = a$  for all  $\sqrt{\delta^T \Sigma^{-1} \delta} \leq \Phi^{-1}(\underline{p}_a)$ .*

See Appendix 7.2 for the proof. In theorem 5.2, we show that a smoothed classifier  $g$  is robust around  $x$  within  $\ell_2$  Mahalanobis distance  $\sqrt{\delta^T \Sigma^{-1} \delta} \leq \Phi^{-1}(p_a)$  where  $\Phi^{-1}$  is inverse of the standard Gaussian CDF. The same result holds if we replace  $p_a$  with lower bound  $\underline{p}_a$ .

## 6 Conclusion

In this work, we study adversarial robustness against evasion attacks, especially for applications where dataset features have to comply certain constraints related to the domain. To the best of our knowledge, there has not been much focus on these types of data for adversarial robustness, and instead most defenses are designed for problems in image domain. However, many security applications, such as malware detection, credit risk prediction, and spam filtering, have different properties compared to image applications. We propose a defense mechanism which uses non-uniform perturbation sets for adversarial training and enables integration of domain expert knowledge. We also show the integration of non-uniform perturbation bounds into certified robustness. Our results on three different applications demonstrate the efficacy of our approach.

## References

Anderson, H. S. and Roth, P. EMBER: an open dataset for training static PE malware machine learning models. *arXiv preprint arXiv: 1804.04637*, 2018.

Ballet, V., Renard, X., Aigrain, J., Laugel, T., Frossard, P., and Detyniecki, M. Imperceptible adversarial attacks on tabular data. *arXiv preprint arXiv:1911.03274*, 2019.

Biggio, B., Corona, I., Maiorca, D., Nelson, B., Šrndić, N., Laskov, P., Giacinto, G., and Roli, F. Evasion attacks against machine learning at test time. In *Joint European conference on machine learning and knowledge discovery in databases*, pp. 387–402. Springer, 2013.

Cohen, J. M., Rosenfeld, E., and Kolter, J. Z. Certified adversarial robustness via randomized smoothing. *arXiv preprint arXiv:1902.02918*, 2019.

DEFCON. *Machine learning static evasion competition*, 2019. URL <https://www.elastic.co/blog/machine-learning-static-evasion-competition>.

Dvijotham, K., Stanforth, R., Gowal, S., Mann, T. A., and Kohli, P. A dual approach to scalable verification of deep networks. In *UAI*, volume 1, pp. 2, 2018.

Fleshman, W. *Evading Machine Learning Malware Classifiers*, 2019. URL <https://towardsdatascience.com/evading-machine-learning-malware-classifiers-ce52dabdb713>.

Gehr, T., Mirman, M., Drachsler-Cohen, D., Tsankov, P., Chaudhuri, S., and Vechev, M. Ai2: Safety and robustness certification of neural networks with abstract interpretation. In *2018 IEEE Symposium on Security and Privacy (SP)*, pp. 3–18. IEEE, 2018.

Goodfellow, I. J., Shlens, J., and Szegedy, C. Explaining and harnessing adversarial examples. *arXiv preprint arXiv:1412.6572*, 2014.

Guo, W., Mu, D., Xu, J., Su, P., Wang, G., and Xing, X. Lemma: Explaining deep learning based security applications. In *Proceedings of the 2018 ACM SIGSAC Conference on Computer and Communications Security, CCS ’18*, pp. 364–379, New York, NY, USA, 2018. Association for Computing Machinery.

Han, J., Kamber, M., and Pei, J. Data transformation and data discretization. *Data Mining: Concepts and Techniques*. Elsevier, pp. 111–118, 2011.

Huang, X. Twiter bot detection, 2017. URL <https://github.com/tapilab/is-xhuang1994>.

Ilyas, A., Santurkar, S., Tsipras, D., Engstrom, L., Tran, B., and Madry, A. Adversarial examples are not bugs, they are features. In *Advances in Neural Information Processing Systems*, volume 32, pp. 125–136. Curran Associates, Inc., 2019.

Kurakin, A., Goodfellow, I., and Bengio, S. Adversarial machine learning at scale. *arXiv preprint arXiv:1611.01236*, 2016.

Lee, K., Eoff, B. D., and Caverlee, J. Seven months with the devils: A long-term study of content polluters on twitter. In *5th International AAAI Conference on Weblogs and Social Media (ICWSM)*, Barcelona, 2011.

Levy, E., Mathov, Y., Katzir, Z., Shabtai, A., and Elovici, Y. Not all datasets are born equal: On heterogeneous data and adversarial examples. *arXiv preprint arXiv:2010.03180*, 2020.

Li, D. and Li, Q. Adversarial deep ensemble: Evasion attacks and defenses for malware detection. *IEEE Transactions on Information Forensics and Security*, 15:3886–3900, 2020.

Liu, C., Tomioka, R., and Cevher, V. On certifying non-uniform bounds against adversarial attacks. In Chaudhuri, K. and Salakhutdinov, R. (eds.), *Proceedings of the 36th International Conference on Machine Learning*, volume 97 of *Proceedings of Machine Learning Research*, pp. 4072–4081, Long Beach, California, USA, 09–15 Jun 2019. PMLR.

Liu, N., Yang, H., and Hu, X. Interpretation to adversary. 2018a. URL <https://github.com/ninghaohello/Interpretation2Adversary>.

Liu, N., Yang, H., and Hu, X. Adversarial detection with model interpretation. In *Proceedings of the 24th ACM SIGKDD International Conference on Knowledge Discovery & Data Mining*, pp. 1803–1811, 2018b.

Lundberg, S. and Lee, S.-I. A unified approach to interpreting model predictions. 12 2017.

Madry, A., Makelov, A., Schmidt, L., Tsipras, D., and Vladu, A. Towards deep learning models resistant to adversarial attacks. *arXiv preprint arXiv:1706.06083*, 2017.

Mahalanobis, P. C. On the generalized distance in statistics. *Proceedings of the National Institute of Sciences*, 2:49–55, 1936.

Merz, C. J. and Murphy, P. *UCI repository of machine learning databases*, 1996. URL <http://www.cs.uci.edu/~mlearn/MLRepository.html>.

Mirman, M., Gehr, T., and Vechev, M. Differentiable abstract interpretation for provably robust neural networks. In *International Conference on Machine Learning*, pp. 3578–3586, 2018.

Pendlebury, F., Pierazzi, F., Jordaney, R., Kinder, J., and Cavallaro, L. {TESSERACT}: Eliminating experimental bias in malware classification across space and time. In *28th {USENIX} Security Symposium ({USENIX} Security 19)*, pp. 729–746, 2019.

Pierazzi, F., Pendlebury, F., Cortellazzi, J., and Cavallaro, L. Intriguing properties of adversarial ml attacks in the problem space. In *2020 IEEE Symposium on Security and Privacy (SP)*, pp. 1332–1349. IEEE, 2020.

Raghunathan, A., Steinhardt, J., and Liang, P. S. Semidefinite relaxations for certifying robustness to adversarial examples. In *Advances in Neural Information Processing Systems*, pp. 10877–10887, 2018.

Rosenberg, I., Meir, S., Berrebi, J., Gordon, I., Sicard, G., and David, E. O. Generating end-to-end adversarial examples for malware classifiers using explainability. In *2020 International Joint Conference on Neural Networks (IJCNN)*, pp. 1–10. IEEE, 2020.

Salman, H., Yang, G., Zhang, H., Hsieh, C.-J., and Zhang, P. Benchmark for lp-relaxed robustness verification of relu-networks. 2019. URL <https://github.com/Hadisalman/robust-verify-benchmark>.

Shapley, L. S. *Notes on the n-Person Game -; II: The Value of an n-Person Game*. RAND Corporation, Santa Monica, CA", 1951.

Singh, G., Gehr, T., Mirman, M., Püschel, M., and Vechev, M. Fast and effective robustness certification. *Advances in Neural Information Processing Systems*, 31:10802–10813, 2018.

Szegedy, C., Zaremba, W., Sutskever, I., Bruna, J., Erhan, D., Goodfellow, I., and Fergus, R. Intriguing properties of neural networks. *arXiv preprint arXiv:1312.6199*, 2013.

Tsipras, D., Santurkar, S., Engstrom, L., Turner, A., and Madry, A. There is no free lunch in adversarial robustness (but there are unexpected benefits). *ArXiv*, abs/1805.12152, 2018.

VirusTotal. URL <http://www.virustotal.com/>.

Wang, S., Chen, Y., Abdou, A., and Jana, S. Mixtrain: Scalable training of formally robust neural networks. *arXiv preprint arXiv:1811.02625*, 14, 2018.

Wong, E. and Kolter, J. Z. Learning perturbation sets for robust machine learning. *arXiv preprint arXiv: 2007.08450*, 2020.

Wong, E. and Kolter, Z. Provably robust neural networks. 2018a. URL [https://github.com/locuslab/convex\\_adversarial](https://github.com/locuslab/convex_adversarial).

Wong, E. and Kolter, Z. Provable defenses against adversarial examples via the convex outer adversarial polytope. In *International Conference on Machine Learning*, pp. 5286–5295. PMLR, 2018b.

Wong, E., Rice, L., and Kolter, J. Z. Fast is better than free: Revisiting adversarial training. *arXiv preprint arXiv:2001.03994*, 2020.

Zeager, M. F., Sridhar, A., Fogal, N., Adams, S., Brown, D. E., and Beling, P. A. Adversarial learning in credit card fraud detection. In *2017 Systems and Information Engineering Design Symposium (SIEDS)*, pp. 112–116. IEEE, 2017.

Zhang, H., Weng, T.-W., Chen, P.-Y., Hsieh, C.-J., and Daniel, L. Efficient neural network robustness certification with general activation functions. In *Advances in neural information processing systems*, pp. 4939–4948, 2018.

## 7 Appendix

### 7.1 Ember Dataset Features

The EMBER dataset Anderson & Roth (2018) consists of two types of features:

1. **Parsed features** are extracted after parsing the portable executable (PE) file. Parsed features include 5 different groups:
  - *General file information*: virtual size of the file; number of imported/exported functions and symbols; whether the file has a debug section, thread local storage, resources, relocations, or a signature.
  - *Header information*: timestamp in the header; target machine; list of image and DLL characteristics; target subsystem; file magic; image, system and subsystem versions; code, headers and commit sizes (hashing trick).
  - *Imported functions*: functions extracted from the import address table (hashing trick)
  - *Exported functions*: list of exported functions (hashing trick).
  - *Section information*: name, size, entropy, virtual size, and a list of strings representing section characteristics (hashing trick).
2. **Format-agnostic features** do not require parsing the PE file structure and include:
  - *Byte histogram*: counts of each byte value within the file (256 integer values).
  - *Byte-entropy histogram*: quantized and normalized of the joint distribution  $p(H, X)$  of entropy  $H$  and byte value  $X$  (256 bins).
  - *String information*: number of strings and their average length; a histogram of the printable characters within those strings; entropy of characters across all printable strings.

### 7.2 Theorem Proofs

**Theorem 3.1.**  $\gamma$ -consistency of the AEs generated under Mahalanobis distance constraint has a direct relation to  $\epsilon$  such that

$$\sqrt{2C - 2 \log \gamma} \leq \epsilon. \quad (18)$$

where  $C = -\log(2\pi)^{d/2} |\Sigma_y|^{1/2}$ ,  $d$  is the dimension of  $x$ , and  $\sqrt{\delta^T \Sigma_y^{-1} \delta} \leq \epsilon$ .

*Proof.* For an AE  $x$  that is generated under the Mahalanobis distance constraint, i.e.,  $x \in (-\delta, +\delta)$ , we can write the following bound:

$$\begin{aligned} \min_{x \in (-\delta, +\delta)} \log \mathbb{P}(X = x | y) &= C - \frac{1}{2} \delta^T \Sigma_y^{-1} \delta \\ &= \log \gamma \end{aligned} \quad (19)$$

where the second equality is a result of  $\gamma$ -consistency assumption. Then, by using the upper limit of  $\ell_2$  Mahalanobis distance of  $\delta$  for  $M = \Sigma_y$ , we get

$$\begin{aligned} \sqrt{\delta^T \Sigma_y^{-1} \delta} &= \sqrt{2C - 2 \log \gamma} \\ &\leq \epsilon. \end{aligned} \quad (20)$$

□

Theorem 3.1 implies that there is a direct relationship between limiting the Mahalanobis distance of  $\delta$  and ensuring consistent samples when the data is Gaussian.

**Theorem 5.1.** *The dual of the linear program 13 can be written as*

$$\begin{aligned}
\underset{\hat{\nu}, \nu}{\text{maximize}} \quad & - \sum_{i=1}^{k-1} \nu_{i+1}^T b_i + \sum_{i=2}^{k-1} \sum_{j \in \mathcal{I}_i} l_{i,j} [\hat{\nu}_{i,j}]_+ - \hat{\nu}_1^T x \\
& - \epsilon \|\Omega^{-1} \hat{\nu}_1\|_q \\
\text{s.t.} \quad & \nu_k = -c \\
& \hat{\nu}_i = (W_i^T \nu_{i+1}), i = k-1, \dots, 1 \\
& \nu_{i,j} = \begin{cases} 0 & j \in \mathcal{I}_i^- \\ \hat{\nu}_{i,j} & j \in \mathcal{I}_i^+ \\ \frac{u_{i,j} - l_{i,j}}{u_{i,j} - l_{i,j}} [\hat{\nu}_{i,j}]_+ - \eta [\hat{\nu}_{i,j}]_- & j \in \mathcal{I}_i \end{cases} \\
& i = k-1, \dots, 2
\end{aligned} \tag{21}$$

where  $\mathcal{I}_i^-$ ,  $\mathcal{I}_i^+$  and  $\mathcal{I}_i$  represent the activation sets in layer  $i$  for  $l$  and  $u$  are both negative, both positive and span zero, respectively.

*Proof.* The linear program with non-uniform input perturbation and relaxed ReLU constraints can be written as

$$\begin{aligned}
\underset{\hat{z}_k}{\text{minimize}} \quad & c^T \hat{z}_k \\
\text{s.t.} \quad & \hat{z}_{i+1} = W_i z_i + b_i, i = 1, \dots, k-1 \\
& \|\Omega(z_1 - x)\|_p \leq \epsilon \\
& z_{i,j} = 0, i = 2, \dots, k-1, j \in \mathcal{I}_i^- \\
& z_{i,j} = \hat{z}_{i,j}, i = 2, \dots, k-1, j \in \mathcal{I}_i^+ \\
& \left. \begin{array}{l} z_{i,j} \geq 0, \\ z_{i,j} \geq \hat{z}_{i,j}, \\ ((u_{i,j} - l_{i,j}) z_{i,j} - u_{i,j} \hat{z}_{i,j}) \leq -u_{i,j} l_{i,j} \end{array} \right\} \begin{array}{l} i=2, \dots, k-1 \\ j \in \mathcal{I}_i \end{array}.
\end{aligned} \tag{22}$$

We associate the following Lagrangian variables with each of the constraints except the  $\ell_p$  norm constraint in Problem 22,

$$\begin{aligned}
& \hat{z}_{i+1} = W_i z_i + b_i \Rightarrow \nu_{i+1} \\
& \delta = z_1 - x \Rightarrow \psi \\
& -z_{i,j} \leq 0 \Rightarrow \mu_{i,j} \\
& \hat{z}_{i,j} - z_{i,j} \leq 0 \Rightarrow \tau_{i,j} \\
& ((u_{i,j} - l_{i,j}) z_{i,j} - u_{i,j} \hat{z}_{i,j}) \leq -u_{i,j} l_{i,j} \Rightarrow \lambda_{i,j}.
\end{aligned} \tag{23}$$

We do not define explicit dual variables for  $z_{i,j} = 0$  and  $z_{i,j} = \hat{z}_{i,j}$  since they will be zero in the optimization. Then, we create the following Lagrangian by grouping up the terms with  $z_i, \hat{z}_i$ :

$$\begin{aligned}
L(\mathbf{z}, \hat{\mathbf{z}}, \nu, \delta, \lambda, \tau, \mu, \psi) = & \psi^T \delta + \psi^T x - (W_1^T \nu_2 + \psi)^T z_1 \\
& - \sum_{\substack{i=2 \\ j \in \mathcal{I}_i}}^{k-1} (\mu_{i,j} + \tau_{i,j} - \lambda_{i,j} (u_{i,j} - l_{i,j}) + (W_i^T \nu_{i+1})_j) z_{i,j} \\
& + \sum_{\substack{i=2 \\ j \in \mathcal{I}_i}}^{k-1} (\tau_{i,j} - \lambda_{i,j} u_{i,j} + \nu_{i,j}) \hat{z}_{i,j} + (c + \nu_k)^T \hat{z}_k \\
& - \sum_{i=1}^{k-1} \nu_{i+1}^T b_i + \sum_{\substack{i=2 \\ j \in \mathcal{I}_i}}^{k-1} \lambda_{i,j} u_{i,j} l_{i,j} \\
\text{subject to} \quad & \|\Omega \delta\|_p \leq \epsilon
\end{aligned} \tag{24}$$

Now, we take the minimum of  $L(\cdot)$  w.r.t  $\mathbf{z}$ ,  $\hat{\mathbf{z}}$  and  $\delta$ :

$$\begin{aligned}
\inf_{\mathbf{z}, \hat{\mathbf{z}}, \delta} L(\cdot) &= \psi^T x - \sum_{i=1}^{k-1} \nu_{i+1}^T b_i + \sum_{\substack{i=2 \\ j \in \mathcal{I}_i}}^{k-1} \lambda_{i,j} u_{i,j} l_{i,j} \\
&+ \inf_{\|\Omega \delta\|_p \leq \epsilon} \psi^T \delta - \inf_{z_1} (W_1^T \nu_2 + \psi)^T z_1 \\
&- \inf_{z_{i,j}} \sum_{\substack{i=2 \\ j \in \mathcal{I}_i}}^{k-1} (\mu_{i,j} + \tau_{i,j} - \lambda_{i,j} (u_{i,j} - l_{i,j}) + (W_i^T \nu_{i+1})_j) z_{i,j} \\
&+ \inf_{\hat{\mathbf{z}}} \left( \sum_{\substack{i=2 \\ j \in \mathcal{I}_i}}^{k-1} (\tau_{i,j} - \lambda_{i,j} u_{i,j} + \nu_{i,j}) \hat{z}_{i,j} + (c + \nu_k)^T \hat{z}_k \right).
\end{aligned} \tag{25}$$

We can represent the term  $\inf_{\|\Omega \delta\|_p \leq \epsilon} \psi^T \delta$  independent of  $\delta$  using the following dual norm definition.

**Cauchy-Schwarz inequality for dual norm:**

We can write the Cauchy-Schwarz inequality as  $\alpha^T \beta \leq \|\alpha\|_p \|\beta\|_q$ , where  $\frac{1}{p} + \frac{1}{q} = 1$  and  $q$  norm represents the dual of  $p$  norm. Let  $\hat{u} = \frac{\alpha}{\|\alpha\|_p}$ , the definition of dual norm is

$$\|\beta\|_q = \sup_{\|\hat{u}\|_p \leq 1} \hat{u}^T \beta. \tag{26}$$

We can write  $\inf_{\|\Omega \delta\|_p \leq \epsilon} \psi^T \delta = -\sup_{\|\Omega \delta\|_p \leq \epsilon} (-\psi^T \delta) = -\sup_{\|\Omega \delta\|_p \leq \epsilon} \psi^T \delta$ . For  $\alpha = \frac{\Omega \delta}{\epsilon}$  and  $\beta = \epsilon \Omega^{-1} \psi$ , we get  $\delta^T \psi \leq \|\frac{\Omega \delta}{\epsilon}\|_p \|\epsilon \Omega^{-1} \psi\|_q$  which implies  $-\sup_{\|\Omega \delta\|_p \leq \epsilon} \psi^T \delta = -\epsilon \|\Omega^{-1} \psi\|_q$ .

Hence, the minimization of  $L(\cdot)$  becomes,

$$\inf_{\mathbf{z}, \hat{\mathbf{z}}, \delta} L(\cdot) = \begin{cases} -\sum_{i=1}^{k-1} \nu_{i+1}^T b_i + \sum_{\substack{i=2 \\ j \in \mathcal{I}_i}}^{k-1} \lambda_{i,j} u_{i,j} l_{i,j} & \text{if cond.} \\ +\psi^T x - \epsilon \|\Omega^{-1} \psi\|_q & \\ -\infty & \text{o.w.} \end{cases} \tag{27}$$

where the conditions are

$$\begin{aligned}
\nu_k &= -c \\
W_1^T \nu_2 &= -\psi \\
\nu_{i,j} &= 0, j \in \mathcal{I}_i^- \\
\nu_{i,j} &= (W_i^T \nu_{i+1})_j, j \in \mathcal{I}_i^+ \\
((u_{i,j} - l_{i,j}) \lambda_{i,j} \\
&\quad - \mu_{i,j} - \tau_{i,j}) = (W_i^T \nu_{i+1})_j \\
\nu_{i,j} &= u_{i,j} \lambda_{i,j} - \tau_{i,j}
\end{aligned} \tag{28}$$

The dual problem can be rearranged and reduced to the standard form

$$\begin{aligned} \underset{\nu, \psi, \lambda, \tau, \mu}{\text{maximize}} \quad & - \sum_{i=1}^{k-1} \nu_{i+1}^T b_i + \psi^T x - \epsilon \|\Omega^{-1} \psi\|_q \\ & + \sum_{i=2}^{k-1} \lambda_i^T (u_i l_i) \end{aligned} \quad (29)$$

$$\text{s.t.} \quad \nu_k = c \quad (30)$$

$$W_1^T \nu_2 = -\psi \quad (31)$$

$$\nu_{i,j} = 0, j \in \mathcal{I}_i^- \quad (32)$$

$$\nu_{i,j} = (W_i^T \nu_{i+1})_j, j \in \mathcal{I}_i^+ \quad (33)$$

$$\begin{aligned} ((u_{i,j} - l_{i,j}) \lambda_{i,j} \\ - \mu_{i,j} - \tau_{i,j}) = (W_i^T \nu_{i+1})_j \end{aligned} \quad \left. \right\} \begin{aligned} i=2, \dots, k-1 \\ j \in \mathcal{I}_i \end{aligned} \quad (34)$$

$$\nu_{i,j} = u_{i,j} \lambda_{i,j} - \tau_{i,j} \quad (35)$$

The insight of the dual problem is that it can also be written in the form of a deep network. Consider the equality constraint 34, the dual variable  $\lambda$  corresponds to the upper bounds in the convex ReLU relaxation, while  $\mu$  and  $\tau$  correspond to the lower bounds  $z \geq 0$  and  $z \geq \hat{z}$ , respectively. By the complementary property, these variables will be zero if the ReLU constraint is non-tight, and non-zero if the ReLU constraint is tight. since the upper and lower bounds cannot be tight simultaneously, either  $\lambda$  or  $\mu + \tau$  must be zero. Hence, at the optimal solution to the dual problem,

$$\begin{aligned} (u_{i,j} - l_{i,j}) \lambda_{i,j} &= [(W_i^T \nu_i + 1)_j]_+ \\ \tau_{i,j} + \mu_{i,j} &= [(W_i^T \nu_i + 1)_j]_- \end{aligned} \quad (36)$$

Combining this with the constraint  $\nu_{i,j} = u_{i,j} \lambda_{i,j} - \tau_{i,j}$  leads to

$$\nu_{i,j} = \frac{u_{i,j}}{u_{i,j} - l_{i,j}} [(W_i^T \nu_i + 1)_j]_+ - \eta [(W_i^T \nu_i + 1)_j]_- \quad (37)$$

for  $j \in \mathcal{I}_i$  and  $0 \leq \eta \leq 1$ . This is a leaky ReLU operation with a slope of  $\frac{u_{i,j}}{u_{i,j} - l_{i,j}}$  in the positive portion and a negative slope  $\eta$  between 0 and 1. Also note that from 31  $-\psi$  denotes the pre-activation variable for the first layer. For the sake of simplicity, we use  $\hat{\nu}_i$  to denote the pre-activation variable for layer  $i$ , then the objective of the dual problem becomes

$$\begin{aligned} S_{D_\epsilon}(x, \nu) &= - \sum_{i=1}^{k-1} \nu_{i+1}^T b_i + \sum_{i=2}^{k-1} \sum_{j \in \mathcal{I}_i} \frac{u_{i,j} l_{i,j}}{u_{i,j} - l_{i,j}} [\hat{\nu}_{i,j}]_+ \\ &\quad - \hat{\nu}_1^T x - \epsilon \|\Omega^{-1} \hat{\nu}_1\|_q \\ &= - \sum_{i=1}^{k-1} \nu_{i+1}^T b_i + \sum_{i=2}^{k-1} \sum_{j \in \mathcal{I}_i} l_{i,j} [\hat{\nu}_{i,j}]_+ \\ &\quad - \hat{\nu}_1^T x - \epsilon \|\Omega^{-1} \hat{\nu}_1\|_q \end{aligned} \quad (38)$$

Hence, the final form of the dual problem can be rewritten as a network with objective  $S_{D_\epsilon}(x, \nu)$ , input  $-c$  and activations  $\mathcal{I}$  as follows:

$$\begin{aligned} \underset{\hat{\nu}, \nu}{\text{maximize}} \quad & - \sum_{i=1}^{k-1} \nu_{i+1}^T b_i + \sum_{i=2}^{k-1} \sum_{j \in \mathcal{I}_i} l_{i,j} [\hat{\nu}_{i,j}]_+ - \hat{\nu}_1^T x \\ & - \epsilon \|\Omega^{-1} \hat{\nu}_1\|_q \\ \text{s.t.} \quad & \nu_k = -c \\ & \hat{\nu}_i = (W_i^T \nu_{i+1}), i = k-1, \dots, 1 \\ & \nu_{i,j} = \begin{cases} 0 & j \in \mathcal{I}_i^- \\ \hat{\nu}_{i,j} & j \in \mathcal{I}_i^+ \\ \frac{u_{i,j}}{u_{i,j} - l_{i,j}} [\hat{\nu}_{i,j}]_+ - \eta [\hat{\nu}_{i,j}]_- & j \in \mathcal{I}_i \end{cases} \\ & i = k-1, \dots, 2 \end{aligned} \quad (39)$$

□

**Theorem 5.2.** In binary classification problem, suppose  $\underline{p}_a \in (\frac{1}{2}, 1]$  satisfies  $\mathbb{P}(f(x+n) = a) \geq \underline{p}_a$ . Then  $g(x+\delta) = a$  for all  $\sqrt{\delta^T \Sigma^{-1} \delta} \leq \Phi^{-1}(\underline{p}_a)$ .

*Proof.* Let  $X$  and  $Y$  be random variables such that  $X \sim \mathcal{N}(x, \Sigma)$  and  $Y \sim \mathcal{N}(x + \delta, \Sigma)$ . Next, we define the set  $\mathcal{A} := \{x \mid \delta^T \Sigma^{-1} (z - x) \leq \sqrt{\delta^T \Sigma^{-1} \delta} \Phi^{-1}(\underline{p}_a)\}$  so that  $\mathbb{P}(X \in \mathcal{A}) = \underline{p}_a$ . It can be shown that  $\mathbb{P}(Y \in \mathcal{A}) = \Phi(\Phi^{-1}(\underline{p}_a) - \sqrt{\delta^T \Sigma^{-1} \delta})$ . To ensure that  $Y$  is classified as class  $A$ , we need

$$\Phi(\Phi^{-1}(\underline{p}_a) - \sqrt{\delta^T \Sigma^{-1} \delta}) \geq 1/2 \quad (40)$$

which can be satisfied if  $\sqrt{\delta^T \Sigma^{-1} \delta} \leq \Phi^{-1}(\underline{p}_a)$ . □

### 7.3 Experiments for Section 4.1

In this section, we present a detailed explanation about the winner attacks Fleshman (2019) of malware competition DEFCON (2019), and show detailed evasion success of these attacks in Table 1.

**GREEDY ATTACK** : Bytes in a range 256 are added iteratively to the malware binaries to make sure the prediction score for a known model lowers and none of the packing, functionality, or anti-tampering checks are affected. Byte addition is stopped when the prediction score gets lower than a threshold value or the file size exceeds 5MB. We generate 1000 adversarial examples from the malicious binaries of EMBER test set for each target model, such as standard trained neural network, adversarially trained model with  $\ell_2$ -PGD for  $\epsilon = 5$  and LGBM model which were provided as benchmark together with EMBER dataset Anderson & Roth (2018); and we call these adversarial example sets GreedyNN, GreedyLGBM and GreedyAdv, respectively.

**CONSTANT PADDING ATTACK** : A new section is created in the binary file and filled with a constant value of size 10000. This attack is applied to 2000 binaries from EMBER malicious test set for constants “169” and “0”, and we call these adversarial example sets C1 Pad. and C2 Pad., respectively.

**STRING PADDING ATTACK** : Strings of size 10000 from a benign file, such as Microsoft’s End User License Agreement (EULA), are added to a new section created in the malware binary. We generate 2000 adversarial examples, which we call set String Pad., by string padding EMBER malicious test set.

Table 1 shows the average number of adversarial examples out of 1000 which successfully evade the corresponding models. While *NU- $\delta$ -Mask* and *NU- $\delta$ -MDtarget* have better performance against Greedy attacks for most of the time, i.e., sets GreedyNN, GreedyLGBM and GreedyAdv, *NU- $\delta$ -Pearson*, *NU- $\delta$ -SHAP* and *NU- $\delta$ -MD* have better accuracy against padding attacks, i.e., sets C1 Pad., C2 Pad. and String Pad.

### 7.4 Experiments for Section 5.1

In this section, we show certification results of adversarially trained models *Uniform- $\delta$*  and *NU- $\delta$ -MDtarget* for spam detection use-case. We consider both uniform and non-uniform input constraints in certification methods namely *Uniform-Cert* for the standard LP approach for certification with uniform perturbation constraint Wong & Kolter (2018b), and *NU-Cert-(.)* for the non-uniform constraint approach that we present in Section 5.1. We implement our non-uniform approach into the LP solution by modifying Wong & Kolter (2018b) with our  $\Omega$  matrix, and generate various certification methods by non-uniform  $\Omega$  selections, e.g. *NU-Cert-SHAP*, *NU-Cert-Pearson*, *NU-Cert-MD* and *NU-Cert-MDtarget*. Our purpose is not to propose the tightest certification bounds but to show that non-uniform input constraint results in larger certification margin compared to the uniform approach. Furthermore, these results support our empirical results in Section 4 where we show adversarial training with non-uniform perturbations provide more robustness than the uniform case.

Since adversarially trained non-uniform approaches in Table 4 have similar performances, we only use *Uniform- $\delta$*  and *NU- $\delta$ -MDtarget* to evaluate certification results. Dropout layers are removed from the model for LP solution, and adversarial training is performed for  $\epsilon = 0.3$ . Certification is done by solving the LP for  $\epsilon = 0.3$  over 1000 spammer test samples. As we mentioned before, the objective should be positive for all classes to certify the corresponding sample. Since our case is binary classification, we only expect the objective of the target class to be positive. The margin between the objective and zero level gives a rough idea about how tight the bound is Salman et al. (2019). To

Method	$\ \delta\ _2$	GreedyNN	GreedyLGBM	GreedyAdv	C1 Pad.	C2 Pad.	String Pad.
Std. Training	-	832	217	337	168	35	123
Uniform- $\delta$	0.1	472.6	105	249.6	66.3	37.6	114.9
NU- $\delta$ -Mask	0.1	408.5	89.2	241.7	46.2	35.2	74.5
NU- $\delta$ -SHAP	0.1	392.8	86.8	206.8	64.9	39	104.7
NU- $\delta$ -Pearson	0.1	417.6	92.8	221.4	45.1	38.2	74.5
NU- $\delta$ -MD	0.1	413	101	216	56	38.7	81.8
NU- $\delta$ -MDtarget	0.1	391.6	84.2	234.6	52.2	38.7	79
Uniform- $\delta$	1	447.2	111.8	273.8	50.1	38.5	83.4
NU- $\delta$ -Mask	1	299.4	88.2	223.4	58.3	40	91
NU- $\delta$ -SHAP	1	359.7	82.2	244.5	53.8	33.6	81.7
NU- $\delta$ -Pearson	1	304	96.2	265	60.5	38.8	99.2
NU- $\delta$ -MD	1	373.2	89.5	244	54.7	37	81.8
NU- $\delta$ -MDtarget	1	360.8	103.4	246.6	45.1	36.7	72.4
Uniform- $\delta$	6.7	231.5	129	333	37.7	38	58.7
NU- $\delta$ -Mask	6.7	104.4	68.4	153.4	43.4	47.3	70.8
NU- $\delta$ -SHAP	6.7	170	113	302.5	32.7	41.2	39.7
NU- $\delta$ -Pearson	6.7	213	78	304	38	38	48.6
NU- $\delta$ -MD	6.7	234	91	314	27.7	31	34.2
NU- $\delta$ -MDtarget	6.7	196	61	301	37.5	33.5	36.5
Uniform- $\delta$	11	177	77.6	278	37.8	41.3	44.6
NU- $\delta$ -Mask	11	94.4	45.2	160.8	30.8	43.7	50.5
NU- $\delta$ -SHAP	11	178	62	296	32	40	35
NU- $\delta$ -Pearson	11	142	75.7	273	31.6	40.7	42.8
NU- $\delta$ -MD	11	195	46	247	40	32.5	43
NU- $\delta$ -MDtarget	11	122.7	44	251.7	34	41	48
Uniform- $\delta$	18	152.2	57.3	234	42.7	51.6	52.3
NU- $\delta$ -Mask	18	44.5	20.2	116.5	27.1	48.2	47.2
NU- $\delta$ -SHAP	18	159.4	48.6	207.2	53.1	59.6	61.3
NU- $\delta$ -Pearson	18	154.2	49	220.4	42.6	61.7	47.2
NU- $\delta$ -MD	18	144.2	49.2	204.6	53	54	63.8
NU- $\delta$ -MDtarget	18	132.4	52.4	215	50.6	53.4	53.2
Uniform- $\delta$	25	233.2	58	228	59.3	51	68.4
NU- $\delta$ -Mask	25	25	14.8	108	21.8	48.9	34.8
NU- $\delta$ -SHAP	25	193.8	53.4	226.2	44.7	56.9	58.7
NU- $\delta$ -Pearson	25	158.2	59.5	191.2	67.6	65.6	75.8
NU- $\delta$ -MD	25	199.7	54	248.5	58.6	59.5	59.7
NU- $\delta$ -MDtarget	25	210	55	225.6	57.7	56.4	60.5

Table 1: **Malware Use-case:** Average number of successful evasions on standard training, uniform and non-uniform  $\ell_2$ -PGD adversarial trainings by the adversarial example sets out of 1000 samples for approximately equal  $\|\delta\|_2$ . Defense success rates shown in Table 2 and Figure 2a are calculated by averaging the success rate over these individual attacks results.

have consistency between the certification methods for the same  $\epsilon$ ,  $\Omega$  matrix for all *NU-Cert-(.)* is scaled such that it has the same norm as  $\Omega = I$  of *Uniform-Cert*.

Table 5 demonstrates two main results: (i) the certification success of *Uniform- $\delta$*  and *NU- $\delta$ -MDtarget* for a single certification method supports our claim that non-uniform perturbations provide higher robustness than uniform approach; and (ii) certification with non-uniform constraints provide larger certification margins and hence tighter bound.

<b>Method</b>	$\ \delta\ _2$	<b>Clean Ac.</b>	<b>Defense S.R.</b>
Std. Training	-	%96.6	%73
Uniform- $\delta$	0.1	%96.2	%82.7 $\pm$ 0.88
NU- $\delta$ -Mask	0.1	%96.2	%85.3 $\pm$ 0.25
NU- $\delta$ -SHAP	0.1	%96.2	%85.2 $\pm$ 0.39
NU- $\delta$ -Pearson	0.1	%96.1	%85.3 $\pm$ 0.94
NU- $\delta$ -MD	0.1	%96.3	%85 $\pm$ 0.99
<b>NU-<math>\delta</math>-MDtarget</b>	0.1	%96.2	<b>%85.4 <math>\pm</math> 0.80</b>
Uniform- $\delta$	1	%96.1	%83.3 $\pm$ 0.41
<b>NU-<math>\delta</math>-Mask</b>	1	%96.1	<b>%86.7 <math>\pm</math> 0.68</b>
NU- $\delta$ -SHAP	1	%96.3	%85.5 $\pm$ 0.61
NU- $\delta$ -Pearson	1	%96.2	%85.7 $\pm$ 0.45
NU- $\delta$ -MD	1	%96.3	%85.4 $\pm$ 0.67
NU- $\delta$ -MDtarget	1	%96.3	%85.9 $\pm$ 0.19
Uniform- $\delta$	6.7	%95.8	%86.3 $\pm$ 0.15
<b>NU-<math>\delta</math>-Mask</b>	6.7	%95.7	<b>%92 <math>\pm</math> 0.07</b>
NU- $\delta$ -SHAP	6.7	%95.8	%88.3 $\pm$ 0.33
NU- $\delta$ -Pearson	6.7	%95.9	%88.2 $\pm$ 0.30
NU- $\delta$ -MD	6.7	%96	%87.7 $\pm$ 0.32
NU- $\delta$ -MDtarget	6.7	%95.8	%89 $\pm$ 0.18
Uniform- $\delta$	11	%95.6	%89.3 $\pm$ 0.54
<b>NU-<math>\delta</math>-Mask</b>	11	%95.8	<b>%92.9 <math>\pm</math> 0.57</b>
NU- $\delta$ -SHAP	11	%96	%90.3 $\pm$ 0.36
NU- $\delta$ -Pearson	11	%95.8	%90 $\pm$ 0.36
NU- $\delta$ -MD	11	%95.9	%89.9 $\pm$ 0.25
NU- $\delta$ -MDtarget	11	%95.7	%90.9 $\pm$ 0.29
Uniform- $\delta$	18	%95.5	%90.17 $\pm$ 0.71
<b>NU-<math>\delta</math>-Mask</b>	18	%95.8	<b>%94.8 <math>\pm</math> 0.51</b>
NU- $\delta$ -SHAP	18	%95.3	%90.45 $\pm$ 0.30
NU- $\delta$ -Pearson	18	%95.3	%90.46 $\pm$ 0.25
NU- $\delta$ -MD	18	%95.4	%90.54 $\pm$ 0.46
NU- $\delta$ -MDtarget	18	%95.4	%90.7 $\pm$ 0.51
Uniform- $\delta$	25	%95.6	%88.4 $\pm$ 0.39
<b>NU-<math>\delta</math>-Mask</b>	25	%95.7	<b>%95.8 <math>\pm</math> 0.21</b>
NU- $\delta$ -SHAP	25	%95.5	%89.5 $\pm$ 0.27
NU- $\delta$ -Pearson	25	%94.9	%89.7 $\pm$ 0.40
NU- $\delta$ -MD	25	%95.2	%88.6 $\pm$ 0.26
NU- $\delta$ -MDtarget	25	%95.2	%89 $\pm$ 0.57

Table 2: **Malware Use-case:** Clean accuracy (Ac.) and defense success rate (S.R.) of standard training, uniform and non-uniform  $\ell_2$ -PGD adversarial trainings with EMBER dataset for approximately equal  $\|\delta\|_2$ . Non-uniform perturbation defense approaches outperform the uniform perturbation for all cases against adversarial attacks.

Method	$\ \delta\ _2$	Clean Ac.	Defense S.R.
Std. Training	-	%69.7	%60
Uniform- $\delta$	0.01	%69	%61.3 $\pm$ 0.40
NU- $\delta$ -SHAP	0.01	%68.3	%61.3 $\pm$ 0.35
<b>NU-<math>\delta</math>-Pearson</b>	0.01	%68.3	<b>%61.9 <math>\pm</math> 0.37</b>
NU- $\delta$ -MD	0.01	%69.6	%61.6 $\pm$ 0.32
<b>NU-<math>\delta</math>-MDtarget</b>	0.01	%69.7	<b>%61.9 <math>\pm</math> 0.30</b>
Uniform- $\delta$	0.1	%67.7	%63.4 $\pm$ 0.31
<b>NU-<math>\delta</math>-SHAP</b>	0.1	%67.1	<b>%64.5 <math>\pm</math> 0.20</b>
NU- $\delta$ -Pearson	0.1	%66.8	%64.3 $\pm$ 0.56
NU- $\delta$ -MD	0.1	%66.7	%64.2 $\pm$ 0.32
<b>NU-<math>\delta</math>-MDtarget</b>	0.1	%66.7	<b>%64.5 <math>\pm</math> 0.41</b>
Uniform- $\delta$	0.3	%66.7	%66.4 $\pm$ 0.22
NU- $\delta$ -SHAP	0.3	%65.8	%67.6 $\pm$ 0.30
NU- $\delta$ -Pearson	0.3	%66	%68 $\pm$ 0.21
NU- $\delta$ -MD	0.3	%66.5	%67.1 $\pm$ 0.64
<b>NU-<math>\delta</math>-MDtarget</b>	0.3	%66.3	<b>%69 <math>\pm</math> 0.32</b>
Uniform- $\delta$	0.5	%66.2	%68 $\pm$ 0.32
NU- $\delta$ -SHAP	0.5	%66.5	%69.7 $\pm$ 0.37
NU- $\delta$ -Pearson	0.5	%65.9	%69.4 $\pm$ 0.27
NU- $\delta$ -MD	0.5	%66.3	%69.2 $\pm$ 0.35
<b>NU-<math>\delta</math>-MDtarget</b>	0.5	%66	<b>%69.8 <math>\pm</math> 0.13</b>
Uniform- $\delta$	0.7	%66.1	%69.6 $\pm$ 0.20
<b>NU-<math>\delta</math>-SHAP</b>	0.7	%65.8	<b>%71.1 <math>\pm</math> 0.57</b>
NU- $\delta$ -Pearson	0.7	%65.6	%71 $\pm$ 0.37
NU- $\delta$ -MD	0.7	%66.4	%70.5 $\pm$ 0.30
NU- $\delta$ -MDtarget	0.7	%65.6	%70.3 $\pm$ 0.30
Uniform- $\delta$	1	%65.3	%70.6 $\pm$ 0.44
<b>NU-<math>\delta</math>-SHAP</b>	1	%64.5	<b>%71.3 <math>\pm</math> 0.32</b>
<b>NU-<math>\delta</math>-Pearson</b>	1	%64.3	<b>%71.3 <math>\pm</math> 0.32</b>
NU- $\delta$ -MD	1	%64.9	%71 $\pm$ 0.37
NU- $\delta$ -MDtarget	1	%65	%71 $\pm$ 0.21

Table 3: **Credit Risk Use-case:** Clean accuracy (Ac.) and defense success rate (S.R.) of standard training, uniform and non-uniform  $\ell_2$ -PGD adversarial trainings with German Credit dataset for approximately equal  $\|\delta\|_2$ . Non-uniform perturbation defense approaches outperform the uniform perturbation for all cases against adversarial attacks.

Method	$\ \delta\ _2$	Clean Ac.	Defense S.R.
Std. Training	-	%94.6	%17.5
Uniform- $\delta$	0.1	%91.1	%34.4 $\pm$ 0.16
NU- $\delta$ -SHAP	0.1	%93.9	%35.3 $\pm$ 0.32
NU- $\delta$ -Pearson	0.1	%94	%36 $\pm$ 0.50.
NU- $\delta$ -MD	0.1	%93.9	%36.7 $\pm$ 0.48
<b>NU-<math>\delta</math>-MDtarget</b>	0.1	%93.9	<b>%38.3 <math>\pm</math> 0.50</b>
Uniform- $\delta$	0.3	%92.6	%58.3 $\pm$ 0.66
NU- $\delta$ -SHAP	0.3	%91.9	%66.5 $\pm$ 0.86
NU- $\delta$ -Pearson	0.3	%91.8	%65 $\pm$ 0.21
<b>NU-<math>\delta</math>-MD</b>	0.3	%91.9	<b>%69.4 <math>\pm</math> 0.25</b>
NU- $\delta$ -MDtarget	0.3	%92	%67.9 $\pm$ 0.25
Uniform- $\delta$	0.5	%91.3	%82.8 $\pm$ 0.46
NU- $\delta$ -SHAP	0.5	%90.9	%86.1 $\pm$ 0.14
<b>NU-<math>\delta</math>-Pearson</b>	0.5	%91.2	<b>%87.3 <math>\pm</math> 0.20</b>
NU- $\delta$ -MD	0.5	%91.1	%85.3 $\pm$ 0.30
NU- $\delta$ -MDtarget	0.5	%91.2	%86.8 $\pm$ 0.28
Uniform- $\delta$	0.7	%91.1	%89.6 $\pm$ 0.48
NU- $\delta$ -SHAP	0.7	%90.5	%90.5 $\pm$ 0.19
<b>NU-<math>\delta</math>-Pearson</b>	0.7	%90.6	<b>%90.7 <math>\pm</math> 0.11</b>
NU- $\delta$ -MD	0.7	%90.5	%89.8 $\pm$ 0.35
NU- $\delta$ -MDtarget	0.7	%90.5	%89.1 $\pm$ 0.18
Uniform- $\delta$	1	%90.5	%87.3 $\pm$ 0.62
NU- $\delta$ -SHAP	1	%89.8	%91.4 $\pm$ 0.62
NU- $\delta$ -Pearson	1	%89.9	%92 $\pm$ 0.53
<b>NU-<math>\delta</math>-MD</b>	1	%89.7	<b>%93.3 <math>\pm</math> 0.30</b>
NU- $\delta$ -MDtarget	1	%89.8	%92.5 $\pm$ 0.64

Table 4: **Spam Detection Use-case:** Clean accuracy and defense success rate of standard training, uniform and non-uniform  $\ell_2$ -PGD adversarial trainings with Twitter Spam dataset for approximately equal  $\|\delta\|_2$ .

Robust model	Clean Ac.	Defense S.R.	Certification Method	Margin	Certification Success
Uniform- $\delta$	%91.56	54.87 $\pm$ 1.1	Uniform-Cert	1.07	347.2 $\pm$ 9.4
			NU-Cert-SHAP	1.84	726.4 $\pm$ 6
			NU-Cert-Pearson	2.04	768 $\pm$ 7.1
			NU-Cert-MD	2.40	802 $\pm$ 5.6
			NU-Cert-MDtarget	2.40	802 $\pm$ 5.5
NU- $\delta$ -MDtarget	%91.4	63.4 $\pm$ 0.74	Uniform-Cert	1.11	429.5 $\pm$ 6.9
			NU-Cert-SHAP	1.9	746.5 $\pm$ 8.5
			NU-Cert-Pearson	2.06	783.8 $\pm$ 7.6
			NU-Cert-MD	2.41	813 $\pm$ 6.8
			NU-Cert-MDtarget	2.41	813 $\pm$ 6.7

Table 5: **Spam Detection Use-case:** Average certification margin and number of successful certified samples out of 1000 spammer samples for *NU- $\delta$ -MDtarget* and *Uniform-Cert*. *NU- $\delta$ -MDtarget* is certifiably robust for more samples than *Uniform- $\delta$*  for all certification methods. For both robust models, certification using non-uniform constraints provide larger certification margins compared to uniform case indicating tighter certification bounds.